Pergamon

Int. J. Heat Mass Transfer. Vol. 38, No. 7, pp. 1173–1185, 1995

0017–9310/95 $9.50+0.00

0017–9310(94)00245–2

Three-dimensional heat and moisture transfer with viscoelastic strain–stress formation in composite food during drying

YOSHINORI ITAYA,† TAKASHI KOBAYASHI‡ and KAN-ICHI HAYAKAWA§

Department of Food Science, New Jersey Agricultural Experiment Station, Cook College, Rutgers University, P.O. Box 231, New Brunswick, NJ 08903, U.S.A.

(*Received* 13 *October* 1993 *and in final form* 27 *July* 1994)

Abstract—A simulation model was developed for three-dimensional heat and moisture transfer and viscoelastic hygrostress formation in a composite body undergoing drying. In the model the chemical potential of moisture in the body was used as a mass transfer potential since different materials had different affinities to moisture. The governing equations were solved numerically by a finite element method. The model was validated experimentally through drying experiments using triply layered brick shaped samples made of the hydrates of starch granules and of 3 : 1 mixture of starch granules and sucrose.

INTRODUCTION

Most foods undergo volumetric changes during the drying process. These changes are accompanied with internal strain–stress formation, resulting in inferior product quality or product loss due to stress-crack formation, without careful process control. Therefore, several researchers have developed methods for simulating heat and moisture transfer and hygrostrain–stress formation in food undergoing drying to assist process optimization and control.

Gustafson *et al.* [1] analyzed heat transfer and elastic stresses in a corn kernel during heating and cooling by a finite element method. Misra and Young [2] simulated moisture diffusion and the elastic shrinkage in spherically approximated soybeans during drying. Tsukada *et al.* [3] developed a computerized method to estimate simultaneous heat and moisture transfer and strain–stress formation in elastoplastic food during drying.

Since many foods are viscoelastic, several researchers determined their viscoelastic properties [4–7]. Hammerle [8] derived an equation to analyze stresses in a viscoelastic slab for known temperature and moisture distributions. Rao *et al.* [9, 10] analyzed the stresses in a viscoelastic cylinder or sphere for assumed moisture and temperature distributions. Litchfield and Okos [11] used Rao *et al.*'s [9] spherical stress equations together with heat and moisture transfer equations to estimate the hygrophysical changes of viscoelastic corn kernels during drying, tempering and cooling processes. Haghighi and Segerlind [12, 13] developed a method for simulating strain–stress formation in a viscoelastic, homogeneous biological material and applied it to analyze thermo-hygrostress formation in an elastic spherical food undergoing drying. Irudayaraj and Haghighi [14] developed a simulation model for heat and moisture and thermo-hygro viscoelastic stress formation in an axisymmetric, heterogeneous body of an arbitrary cross-sectional contour (a two-dimensional problem). They assumed implicitly homogeneous hygrochemical affinities for all heterogeneous components since moisture concentration was used as a moisture transfer potential although heterogeneous viscoelastic properties were assumed. Irudayaraj *et al.* [15] applied the developed method to analyze drying processes of soybeans and corn kernels.

Many foods are irregular and nonhomogeneous. Within such foods, heat and moisture transfer and strain–stress formation are three-dimensional. Furthermore, one needs to consider the interactive influence of nonhomogeneity on heat and moisture transfer as well as on strain–stress formation since different components have different affinities to water. However, virtually all published papers are for homogeneous and one- or two-dimensional transport processes.

The objective of this work is to develop a method for predicting three-dimensional heat and moisture transfer with viscoelastic strain–stress formation in a composite food during drying.

THEORY

Heat and moisture transfer

Simultaneous, transient state heat and moisture transfer in food is simulated using a modified Luikov's

† Present address: Department of Chemical Engineering, Nagoya University, Nagoya 464, Japan.

‡ Present address: Aomori Polytechnical College, Iizume, Goshyogawara City, Aomori 037, Japan.

§ Author to whom correspondence should be addressed.

NOMENCLATURE

- $\mathbf{A}$ deplacement–strain matrix defined by equation (32) [m^{-1}]
- $\mathbf{A}^d$ dimensionless matrix corresponding to $\mathbf{A}$
- $\mathbf{A}_{MM}$ matrix defined by equation (A1)
- $\mathbf{A}_{MT}$ matrix defined by equation (A2)
- $\mathbf{A}_{TM}$ matrix defined by equation (A3)
- $\mathbf{A}_{TT}$ matrix defined by equation (A4)
- a_M moisture shift factor
- a_T temperature shift factor
- a_w water activity
- $\mathbf{B}^d$ strain–nodal displacement matrix defined by equation (56)
- $\mathbf{B}_{MM}$ matrix defined by equation (A4)
- $\mathbf{B}_{MT}$ matrix defined by equation (A5)
- $\mathbf{B}_{TM}$ matrix defined by equation (A7)
- $\mathbf{B}_{TT}$ matrix defined by equation (A8)
- C volumetric moisture concentration [$kg\ m^{-3}$]
- $\mathbf{C}$ matrix defined by equation (30)
- $\mathbf{C}^*$ vector defined by equation (30)
- C_m $(\partial W/\partial \phi)_T$, specific mass capacity [g water (g dry matter)$^{-1}$M^{-1}]
- C_{MM} coefficient defined by equation (41)
- C_{MT} coefficient defined by equation (41)
- c_p specific heat [$kJ\ kg^{-1}\ K^{-1}$]
- C_T $(\partial W/\partial T)_\phi$, temperature coefficient [g water (g dry matter)$^{-1}$ K^{-1}]
- C_{TM} coefficient defined by equation (41)
- C_{TT} coefficient defined by equation (41)
- $\mathbf{D}_p$ anisotropic pressure mass diffusivity [s]
- $\mathbf{D}_t$ anisotropic Soret mass diffusivity [$kg\ m^{-1}\ s^{-1}\ K^{-1}$]
- $\mathbf{D}_w$ anisotropic moisture diffusivity [$m^2\ s^{-1}$]
- $\mathbf{d}$ nodal displacement vector
- E constant in Gugenheim–Anderson–deBore isotherm formula
- F_i components of body force vector [$Pa\ m^{-1}$]
- Fo $\alpha_r t/l^2$, reference Fourier number
- $\mathbf{F}_M$ moisture flux vector defined by equation (A9)
- $\mathbf{F}_T$ heat flux vector defined by equation (A10)
- G shear modulus [Pa]
- $G_1(t)$ shear modulus relaxation function [Pa]
- $G_{1d}(Fo)$ function obtained replacing t in $G_1(t)$ by $Fo\ l^2/\alpha_r$ [Pa]
- G_1^r reference shear modulus relaxation value normally G_1 (0)
- $G_2(t)$ bulk modulus relaxation function [Pa]
- $G_{2d}(Fo)$ function obtained replacing t in $G_2(t)$ by $Fo\ l^2/\alpha$ [Pa]
- G_{ijkl} elements of material properties tensor denied by equation (22) [Pa]
- ΔG° Gibbs' free energy of saturated, liquid water [$J\ mol^{-1}$]
- H high amylose starch granules hydrate
- H_M mass transfer Biot number defined by equation (43)
- H_T heat transfer Biot number defined by equation (43)
- HSH triply layered composite brick shaped sample with one layer of S between two layers of H
- ΔH° enthalpy of saturated liquid water [$J\ mol^{-1}$]
- ΔH_{rj} reaction heat of jth chemical reaction [$J\ kg^{-1}$]
- ΔH_{rj}^d dimensionless reaction heat defined by equation (43)
- ΔH_v latent heat of moisture vaporization or condensation [$J\ kg^{-1}$]
- ΔH_v^d dimensionless latent heat defined by equation (43)
- h_m mass transfer coefficient [$kg\ m^{-2}\ Pa^{-1}\ s^{-1}$]
- h_t heat transfer coefficient [$W\ m^{-2}\ k^{-1}$]
- $\mathbf{J}_h$ heat flux [$W\ m^2$]
- $\mathbf{J}_m$ moisture flux [$kg\ m^{-2}\ s^{-1}$]
- K bulk modulus [Pa]
- $\mathbf{k}_c$ anisotropic Dufour thermal conductivity [$W\ m^2\ kg^{-1}$]
- $\mathbf{K}^d$ stiffness matrix defined by equation (57)
- $\mathbf{K}_{MM}$ matrix defined by equation (42)
- $\mathbf{K}_{MT}$ matrix defined by equation (42)
- $\mathbf{K}_{TM}$ matrix defined by equation (42)
- $\mathbf{K}_{TT}$ matrix defined by equation (42)
- $\mathbf{k}_p$ anisotropic filtration thermal conductivity [$W\ m^{-1}\ kg^{-1}$]
- $\mathbf{k}_t$ anisotropic thermal conductivity [$W\ m^{-1}\ K^{-1}$]
- Le Luikov number defined by equation (43)
- l characteristic dimension [m]
- $\mathbf{N}$ shape function matrix
- $\mathbf{n}$ outward normal unit vector
- n_e number of finite elements used to map food volume
- n_s power for converting S_v to stress free strain element [−]
- p water vapor pressure equilibrated to exposed food surface moisture and temperature, $a_w p_s$ [Pa]
- p_a water vapor pressure of air [Pa]
- p_s saturation water vapor pressure [Pa]
- Q constant in Gugenheim–Anderson–de Bore isotherm formula
- R_j reaction rate [$kg\ s^{-1}\ m^{-3}$]
- $\mathbf{R}^d$ force vector defined by equation (59)
- R gas constant [$J \cdot K^{-1}\ mol^{-1}$]
- S surface variable or hydrate of high amylose starch granules–sucrose 3 : 1 mixture
- S_a surface exposed to atmosphere

S_i	interface between two components
S_v	volumetric shrinkage coefficient
SHS	triply layered brick shaped sample with one layer of H between two layers of S
ΔS^o	molar entropy of pure water [J mol^{-1} K^{-1}]
T	temperature [K]
t	time [s]
$\mathbf{U}$	displacement vector [m]
U_i	element of displacement vector [m]
v	volumetric variable [m^3]
V^d	dimensionless volumetric variable
V	space occupied by food except its exposed surface
v_T	total volume occupied by food
W	moisture content [kg water/kg dry solid]
W_m	moisture content of food equilibrated to 100% humidity [kg water/kg dry solid]
W_n	empirical constant in GAB formula [kg water/kg dry solid]
W_z	moisture content of food equilibrated to 0% humidity [kg water/kg dry solid]
$\mathbf{x}$	dimensional coordinate vector [m]
$\mathbf{X}$	dimensionless coordinate vector [−]
X, Y, Z	dimensionless coordinates. $X = x/l$, $Y = y/l$ and $Z = z/l$.

Greek symbols

α_r	$k_t^r/(c_p \rho_s)$, reference thermal diffusivity
β	Stefan–Boltzman constant [W m^{-2} K^{-4}]
β^d	coefficient defined by equation (43)
Γ	functional defined by equation (56)
γ_1	flux correction factor [m^3 Pa kg^{-1}]
γ_2	flux correction factor [Pa]
γ_{2v}	$\gamma_2\,(\partial S_v/\partial c)$
γ_3	flux correction factor [Pa K^{-1}]
$\boldsymbol{\varepsilon}^s$	initial strain (stress free shrinkage strain) tensor
$\boldsymbol{\varepsilon}$	strain tensor
ε^s	$S_{v_s}^n$
ε_L	Luikov's phase change criterion
ε_{kl}	element of strain tensor
ε_{kl}^s	element of stress free shrinkage strain tensor (strain for stress free deformation)
λ	reduced time defined by equation (24) [s]
μ	chemical potential [J mol^{-1}]
ξ	dummy variable
ρ_b	density of material as is [kg m^{-3}]
ρ_s	density of dry porous solid [kg m^{-3}]
$\boldsymbol{\sigma}$	stress [Pa]
θ	$(T-T^r)/T_a-T^r)$, dimensionless temperature
τ	dimensionless time
Φ	$(\phi-\phi^r)/(\phi_a-\phi^r)$, dimensionless mass transfer potential
ϕ	mass transfer potential, symbol M is used to represent the unit of the potential [M]
ϕ_r	product of radiative adsorptivity and shape factor
φ	relative humidity
ψ	dimensionless equilibrium vapor pressure.

Superscripts

d	dimensionless
n	value at Fo_n
n+1	value at Fo_{n+1}
r	reference property
T	transpose of matrix.

Subscripts

a	atmosphere or equilibration to surrounding air (e.g. ϕ_a is ϕ of food equilibrated to air)
o	initial condition
i, j	dummy subscripts representing x, y, z, xx, yy, zz, xy, yz or zx
k, l	dummy subscripts representing x, y or z
m, n, n+1	numbers of time increments
s	exposed surface
X, Y, Z	X, Y and Z directions or components
α, β	components.

model [16], equations (1) and (2)

$$c_p\rho_b\,\partial T/\partial t = -\mathrm{div}\,(\mathbf{J}_h)+\Sigma_j\Delta H_{rj}R_j+\Delta H_v\varepsilon_L\,\partial c/\partial t \qquad t>0 \quad \mathbf{x}\in V \qquad (1)$$

$$\partial c/\partial t = -\mathrm{div}\,(\mathbf{J}_m)+\Sigma R_j \qquad t>0 \quad \mathbf{x}\in V. \qquad (2)$$

The second term on the right hand side of equation (1) is heat generation or dissipation due to chemical reactions and the third term is latent heat for vaporization or condensation. The second term in equation (2) is a moisture source or sink due to chemical reactions. Fluxes $\mathbf{J}_h$ and $\mathbf{J}_m$ in equations (1) and (2) are expressed as follows for a homogeneous anisotropic food

$$\mathbf{J}_h = -\mathbf{k}_t\cdot\mathrm{grad}\,(T)-(-1)^m\mathbf{k}_c\cdot\mathrm{grad}\,(C) -(-1)^n\mathbf{k}_p\cdot\mathrm{grad}\,(p) \qquad (3)$$

$$\mathbf{J}_m = -\mathbf{D}_w\cdot\mathrm{grad}\,(C)-\mathbf{D}_t\cdot\mathrm{grad}\,(T)-\mathbf{D}_p\cdot\mathrm{grad}\,(p) \qquad (4)$$

where $\mathbf{k}_t$, $\mathbf{k}_c$ and $\mathbf{k}_p$ are anisotropic (orthorhombic) thermal conductivity, Dufour thermal conductivity and filtration thermal conductivity, respectively, $\mathbf{D}_w$,

$\mathbf{D}_t$ and $\mathbf{D}_p$ are anisotropic mass diffusivity, Soret mass diffusivity and pressure mass diffusivity, respectively.

Luikov [17] treated pressure p as a dependent variable together with T and C, resulting in three simultaneous equations for the simulation. However, variable p was eliminated in the above model since it is related to local moisture vaporization or condensation shrinkage and temperature, equation (5)

$$\operatorname{grad}(P) = (\gamma_1\varepsilon_L - \gamma_2\,\partial S_v/\partial C)\operatorname{grad}(C) + \gamma_3\operatorname{grad}(T)$$
$$= (\gamma_1\varepsilon_L - \gamma_{2v})\operatorname{grad}(C) + \gamma_3\operatorname{grad}(T). \quad (5)$$

The initial and boundary conditions are:

I.C.

$$C = C_0,\ T = T_0 \text{ when } t = 0 \text{ and } \mathbf{x}\in S_a \,\&\, V \quad (6)$$

B.C. for surface of material

$$h_t(T_a - T) + \beta\phi_r(T_a^4 - T^4) - h_m(1-\varepsilon)\Delta H_v(p - p_a) = \mathbf{J}_h\cdot\mathbf{n} \quad (7)$$

$$h_m(p - p_a) = \mathbf{J}_m\cdot\mathbf{n}$$
$$\text{where } t > 0 \text{ and } \mathbf{x}\in S_a. \quad (8)$$

The volumetric concentration of moisture, C, is used in the governing equations given above. Therefore, they are not applicable to nonhomogeneous food, whose components have different chemical affinities to water. Luikov [17] used a mass transfer potential derived from normalized moisture sorption isotherms of filter paper. Since this potential did not properly account for the influence of temperature on the mass transfer potential, the chemical potential of water in each component was used as a mass transfer potential ϕ [18]:

$$\phi = \begin{cases} \mu_0 + RT\ln(a_w) & \text{for } W < W_m \\ (W - W_m)/(W_m - W_z)\mu_0 + \mu_0 & \text{for } W_m < W \end{cases} \quad (9)$$

where μ_0 is the chemical potential of saturated liquid water, equation (10):

$$\mu_0 = \Delta G^\circ = \Delta H^\circ - T\Delta S^\circ. \quad (10)$$

Water activity, a_w, may be related to dried mass based moisture concentration W using any reliable moisture sorption isotherm formula (equilibrium assumed between adsorbed moisture in food and vapor in pores within a minute volumetric element). For the present work, Gugenheim–Anderson–deBor (GAB) formula was used since this estimated accurately the isotherms of many dried foods [19]

$$W = W_n EQa_w/\{(1 - Qa_w)(1 - Qa_w + EQa_w)\}. \quad (11)$$

Equations (9)–(11) show W dependent on ϕ and T. Therefore, one has

$$\mathrm{d}W = (\partial W/\partial\phi)_T\mathrm{d}\phi + (\partial W/\partial T)_\phi\,\mathrm{d}T = C_m\,\mathrm{d}\phi + C_T\,\mathrm{d}T. \quad (12)$$

W is related to volumetric concentration C

$$W = C/\rho_s = CS_v/\rho_{so}. \quad (13)$$

Substituting equations (9) and (11)–(13) into equations (1)–(5), the governing equations were transformed as follows

$$\{C_p\rho_s - \Delta H_v\varepsilon_L(\rho_s + \partial\rho_s/\partial W\cdot W)C_T\}\,\partial T/\partial t - \Delta H_v\varepsilon_L(\rho_s + \partial\rho_s/\partial W\cdot W)C_m\,\partial\phi/\partial t = -\operatorname{div}(\mathbf{J}_h) + \Sigma\Delta H_r R_j \quad (14)$$

$$(\rho_s + W\cdot\partial\rho_s/\partial W)(C_m\,\partial\phi/\partial t + C_T\,\partial T/\partial t) = -\operatorname{div}(\mathbf{J}_m) + \Sigma R_j \quad (15)$$

$$\mathbf{J}_h = -\left[\mathbf{k}_t + (-1)^n\gamma_3\mathbf{k}_p + \{(-1)^m\mathbf{k}_c + (-1)^n\mathbf{k}_p \times (\gamma_1\varepsilon_L - \gamma_2')\}\left(\rho_s + \frac{\partial\rho_s}{\partial W}W\right)C_T\cdot\right]\operatorname{grad}(T)$$
$$-\left[\{(-1)^m\mathbf{k}_c + (-1)^n\mathbf{k}_p(\gamma_1\varepsilon_L - \gamma_2')\} \times \left(\rho_s + \frac{\partial\rho_s}{\partial W}W\right)C_m\right]\cdot\operatorname{grad}(\phi) \quad (16)$$

$$\mathbf{J}_m = -\left[\rho_s + \frac{\partial\rho_s}{\partial W}W\{D_w + \left(\gamma_1\varepsilon_L - \gamma_2'\right)\mathbf{D}_p\}C_T + \left(\mathbf{D}_t + \mathbf{D}_p\gamma_3\right)\right]\cdot\operatorname{grad}(T) - \left[\left(\rho_s + \frac{\partial\rho_s}{\partial W}W\right) \times \{\mathbf{D}_w + (\gamma_1\varepsilon_L - \gamma_2')\mathbf{D}_p\}C_m\right]\cdot\operatorname{grad}(\phi). \quad (17)$$

The initial and boundary conditions, equations (6)–(8), are transformed through similar substitution.

Conditions on the interface between two different components α and β are

$$\left.\begin{aligned} T_\alpha &= T_\beta \\ \mathbf{J}_{k\alpha}\cdot\mathbf{n}_\alpha &= \mathbf{J}_{h\beta}\cdot\mathbf{n}_\beta \end{aligned}\right\} \text{ when } t > 0 \text{ and } \mathbf{x}\in S_i \quad (18)$$

$$\left.\begin{aligned} \phi_\alpha &= \phi_\beta \\ J_{m\alpha}\cdot\mathbf{n}_\alpha &= \mathbf{J}_{m\beta}\cdot\mathbf{n}_\beta \end{aligned}\right\} \text{ when } t > 0 \text{ and } \mathbf{x}\in S_i. \quad (19)$$

Viscoelastic strain–stress

Linear viscoelasticity is assumed since it has been used successfully simulating strain–stress formation in many biomaterials [20]. The following are equations expressed in the three-dimensional Cartesian coordinates.

Constitutive equations:

$$\sigma_{ij} = \int_0^t G_{ijk\ell}\{\lambda(t) - \lambda(\xi)\}\{\partial[\varepsilon_{k\ell}(\xi) - \varepsilon_{k\ell}^s\,\varepsilon(\xi)]/\partial\xi\}\,\mathrm{d}\xi. \quad (20)$$

In the above, ξ is a dummy integration variable and t is any time value representing a current drying time.

Using a convolution expression, equation (20) is rewritten as

$$\sigma_{ij} = G_{ijkl} * (\varepsilon_{k\ell} - \varepsilon^{s}_{k\ell}) \tag{21}$$

where

$$G_{ijkl}(t) = (1/3)[G_2(t) - G_1(t)]\delta_{ij}\delta_{kl} + (1/2)G_1(t)[\delta_{ik}\delta_{j\ell} + \delta_{i\ell}\delta_{jk}] \tag{22}$$

$$G(t) = G_1(t)/2, K(t) = G_2(t)/3 \tag{23}$$

G and K are shear and bulk moduli, respectively. λ is the reduced time to account for temperature and moisture dependency of stress by extending or reducing the effective time as defined below [12]

$$\lambda(t) = t/\{a_T(T)a_M(w)\} \tag{24}$$

where a_T and a_M are temperature and moisture shift factors, respectively.

Equilibrium equation:

$$\sigma_{ij,j} + F_i = 0 \tag{25}$$

where $\sigma_{ij,j}$ denotes differentiation of σ_{ij} with respect to j and F_i is a body force vector element

$$\varepsilon_{ij} = (1/2)(U_{i,j} + U_{j,i}). \tag{26}$$

Virtual work. The above given equations describe strain–stress behavior at any one location. To solve these equations, an integrated expression applicable to an entire body is required. This is a functional Γ, virtual work of a deforming body. When there is no body force applied, one has

$$\Gamma = \frac{1}{2}\int_v [G_{ijkl} * \varepsilon_{ij} * \varepsilon_{k\ell} - G_{ijkl} * \varepsilon^{s}_{ij} * \varepsilon_{kl}]\,dv. \tag{27}$$

A governing equation is obtained by minimizing functional $\Gamma(\delta\Gamma = 0)$.

For an isotropic body, equation (27) reduces to as follows with the vectorial representation of strain tensor $\boldsymbol{\varepsilon}$

$$\Gamma = \frac{1}{2}\int_v [C_{ij} * \varepsilon_i * \varepsilon_j - C^{*}_{i} * \varepsilon^{s}_{i} * \varepsilon_i]\,dv \tag{28}$$

$$\boldsymbol{\varepsilon} = \mathbf{AU} \tag{29}$$

where

$$\mathbf{C} = \begin{bmatrix} K+4G/3 & K-2G/3 & K-2G/3 & 0 & 0 & 0 \\ K-2G/3 & K+4G/3 & K-2G/3 & 0 & 0 & 0 \\ K-2G/3 & K-2G/3 & K+4G/3 & 0 & 0 & 0 \\ 0 & 0 & 0 & G & 0 & 0 \\ 0 & 0 & 0 & 0 & G & 0 \\ 0 & 0 & 0 & 0 & 0 & G \end{bmatrix}$$

$$\mathbf{C}^{*} = \begin{Bmatrix} 3K \\ 3K \\ 3K \\ G \\ G \\ G \end{Bmatrix}. \tag{30}$$

$$\boldsymbol{\varepsilon} = \begin{Bmatrix} \varepsilon_x \\ \varepsilon_y \\ \varepsilon_z \\ \varepsilon_{xy} \\ \varepsilon_{yz} \\ \varepsilon_{zx} \end{Bmatrix} \quad \boldsymbol{\varepsilon}^{s} = \begin{Bmatrix} \varepsilon^{s} \\ \varepsilon^{s} \\ \varepsilon^{s} \\ 0 \\ 0 \\ 0 \end{Bmatrix} \quad \varepsilon^{s}_{0} = S^{n_s}_{v} \text{ for } i = 1, 2 \text{ and } 3 \tag{31}$$

$$\mathbf{A} = \begin{bmatrix} \partial/\partial x & 0 & 0 \\ 0 & \partial/\partial y & 0 \\ 0 & 0 & \partial/\partial z \\ (1/2)\partial/\partial y & (1/2)\partial/\partial x & 0 \\ 0 & (1/2)\partial/\partial z & (1/2)\partial/\partial y \\ (1/2)\partial/\partial z & 0 & (1/2)\partial/\partial x \end{bmatrix}$$

$$\mathbf{U} = \begin{Bmatrix} U_x \\ U_y \\ U_z \end{Bmatrix} \tag{32}$$

In equation (31) $\boldsymbol{\varepsilon}^{s}$ is the initial strain and S_v is a volumetric shrinkage function determined through a stress-free drying experiment (uniform moisture distribution in a sample body throughout drying). For the present study, negligible thermal strains were assumed because of negligible thermal expansion of most food.

When the vectorially expressed strain tensor $\boldsymbol{\varepsilon}$ is used, the constitutive equations (21) and (22) become as follows

$$\sigma_i = G_{ik} * (\varepsilon_k - \varepsilon^{s}_{k}) \tag{33}$$

where

$$G_{ik} = C_{ik}. \tag{34}$$

Dimensionless model

The following dimensionless equations are obtained through the dimensional analysis of the above heat and moisture transfer and viscoelastic strain–stress equations.

Heat and moisture transfer:

$$C_{TT}\frac{\partial\theta}{\partial Fo} = C_{TM}\frac{\partial\Phi}{\partial Fo} + \mathrm{div}\,(\mathbf{J}_{TT}) + \mathrm{div}\,(\mathbf{J}_{TM}) + \sum_j \Delta H^{d}_{rj} R^{d}_{j} \tag{35}$$

$$c_{MM}\frac{\partial\Phi}{\partial Fo} = -C_{MT}\frac{\partial\theta}{\partial Fo} + \mathrm{div}\,(\mathbf{J}_{MT}) + \mathrm{div}\,(\mathbf{J}_{MM}) + \sum_j R^{d}_{j} \tag{36}$$

$$\begin{aligned} \mathbf{J}_{TT} &= \mathbf{K}_{TT}\cdot \mathrm{grad}\,(\theta), & \mathbf{J}_{TM} &= \mathbf{K}_{TM}\cdot \mathrm{grad}\,(\Phi) \\ \mathbf{J}_{MT} &= \mathbf{K}_{MT}\cdot \mathrm{grad}\,(\theta), & \mathbf{J}_{MM} &= \mathbf{K}_{MM}\cdot \mathrm{grad}\,(\Phi). \end{aligned} \tag{37}$$

Initial condition:

$$\Phi = \Phi_0 \text{ and } \theta = \theta_0, \quad \text{when } Fo = 0 \text{ and } \mathbf{X} \in S_a \text{ and } V. \tag{38}$$

Boundary conditions:
when $Fo > 0$ and $\mathbf{X} \in S_a$

$$(H_T+\beta^d)(\theta_a-\theta)-(1-\varepsilon_L)H_M\Delta H_v^d(\psi-\psi_a) = \mathbf{J}_{TT}\cdot\mathbf{n}+\mathbf{J}_{TM}\cdot\mathbf{n}$$

$$H_M(\psi-\psi_a) = \mathbf{J}_{MT}\cdot\mathbf{n}+\mathbf{J}_{MM}\cdot\mathbf{n} \tag{39}$$

when $Fo > 0$ and $\mathbf{X} \in S_i$

$$\theta_\alpha = \theta_\beta, \quad \mathbf{J}_{TT}\cdot\mathbf{n}_\alpha = \mathbf{J}_{TT}\cdot\mathbf{n}_\beta$$
$$\Phi_\alpha = \Phi_\beta, \quad \mathbf{J}_{MM}\cdot\mathbf{n}_\alpha = \mathbf{J}_{MM}\cdot\mathbf{n}_\beta \tag{40}$$

where

$$\left.\begin{aligned} C_{TT} &= (C_p/C_p^r)(\rho_b/\rho_s^r)-\frac{\Delta H_v^d}{Le}\varepsilon_L\rho_s^dC_T(T_a-T^r),\\ C_{TM} &= \frac{\Delta H_v^d}{Le}\varepsilon_L\rho_s^dC_m(\phi_a-\phi^r)\\ C_{MM} &= \rho_s^dC_m(\phi_a-\phi^r)/Le, C_{MT} = \rho_s^dC_T(T_a-T^r)/Le \end{aligned}\right\} \tag{41}$$

$$\left.\begin{aligned} \mathbf{K}_{TT} &= [\{\mathbf{k}_t+(-1)^n\gamma_3\mathbf{k}_p\}/K_T^r]\\ &\quad+[\{(-1)^m\mathbf{k}_c+(-1)^n\mathbf{k}_p(\gamma_1\varepsilon_L-\gamma_2')\}/K_T^r]\rho_s^r\rho_s^dC_T\\ \mathbf{K}_{TM} &= [\{(-1)^m\mathbf{k}_c+(-1)^n\mathbf{k}_p(\gamma_1\varepsilon_L-\gamma_2')\}/\\ &\quad k_T]\rho_s^r\rho_s^rC_m^d(\phi_a-\phi^r)/(T_a-T^r)\\ \mathbf{K}_{MM} &= [\{\mathbf{D}_w+\mathbf{D}_p(\gamma_1\varepsilon_L-\gamma_2')\}/D_w^r]\rho_s^dC_m(\phi_a-\phi^r)\\ \mathbf{K}_{MT} &= [\{\mathbf{D}_w+\mathbf{D}_p(\gamma_1\varepsilon_L-\gamma_2')\}/D_w^r]\rho_s^dC_T(T_a-T^r)\\ &\quad+[\{(\mathbf{D}_t+\mathbf{D}_p\gamma_3)/D_w^r\}(T_a-T^r)]/\rho_s^r \end{aligned}\right\} \tag{42}$$

$$\left.\begin{aligned} &H_T = h_tl/k_t^r, \quad H_M = lp_ah_m/(D_w^r\rho_s^r), \quad \psi = p/p^r\\ &Le = D_w^rc_p^r\rho_s^r/k_t^r, \quad R_j^d = l^2R_j/D_w^r\rho_s^r\\ &\Delta H_{rj}^d = D_w^r\rho_s^r\Delta H_{rj}/k_t^r(T_a-T^r)\\ &\Delta H_v^d = D_w^r\rho_s^r\Delta H_v/k_t^r(T_a-T^r)\\ &\rho_s^d = (\rho_s+W\partial\rho_s/\partial W)/\rho_s^r\\ &\beta^d = \frac{\beta\phi^rl(T_a-T^r)^3}{k_t^r}\left\{\left(1+\frac{T^r}{T_a-T^r}\right)^2\right.\\ &\qquad\left.+\left(\theta+\frac{T^r}{T_a-T^r}\right)^2\right\}\left(\theta+\frac{T^r}{T_a-T^r}\right) \end{aligned}\right\}. \tag{43}$$

In the above, θ, Φ and Fo are dimensionless temperature, dimensionless mass transfer potential and reference Fourier number, respectively. $\mathbf{K}_{TT}$, $\mathbf{K}_{TM}$, $\mathbf{K}_{MT}$ and $\mathbf{K}_{MM}$ are dimensionless matrices of orthorhombic thermal conductivity, Dufour thermal conductivity, mass diffusivity and Soret mass diffusivity, respectively. C_{TT}, C_{TM}, C_{MM} and C_{MT} are dimensionless temperature coefficient, latent heat, specific mass capacity and heat and mass interactive coefficient, respectively.

Stress–strain:

$$\sigma_i^d = \frac{\sigma_i}{G_1^r} = \int_0^{Fo} G_{ik}^d(\lambda^d(Fo) - \lambda^d(\xi))\frac{\partial}{\partial\xi}[\varepsilon_k^d(\xi)-\varepsilon_k^{sd}(\xi)]\,d\xi = G_{ik}^d*(\varepsilon_k^d-\varepsilon_k^{sd}) \tag{44}$$

$$G_{ik}^d = G_{ik}/G_1^r \tag{45}$$

$$G^d(Fo) = G(Fo)/G_1^r = G_1(Fo)/(2G_1^r),$$
$$K^d(Fo) = K(Fo)/G_1^r = (1/3)G_2(Fo)/G_1^r \tag{46}$$

$$\lambda^d(Fo) = Fo/\{a_T(\theta)a_M(\phi)\} \tag{47}$$

$$\Gamma^d = \Gamma/\{G_1^rl^3\} = 1/2\int_{v_t^d}[C_{ij}*\varepsilon_i^d*\varepsilon_j-C_i^{*d}*\varepsilon_i^s*\varepsilon_j]\,dv^d$$

(48)$\mathbf{c}^d$ and $\mathbf{c}^{*d}$ are obtained by replacing K and G in equation (32) by K^d and G^d, respectively. Although $\boldsymbol{\varepsilon}$ is dimensionless, it is transformed to ε^d

$$\boldsymbol{\varepsilon}^d = \mathbf{A}^d\cdot\mathbf{U}^d. \tag{49}$$

A^d is obtained by replacing x, y and z of $\mathbf{A}$, equation (32), to corresponding dimensionless location variables and $\mathbf{U}^d$ by replacing its components, equation (32), with those expressed in the dimensionless variables.

Transient state hygroviscoelastic stresses at any drying time may be estimated as follows. One obtains first instantaneous temperature and mass transfer potential distributions. From these distributions, one determines an instantaneous, free shrinkage strain $\boldsymbol{\varepsilon}^{sd}$, distribution, a corresponding hygrostrain, $\boldsymbol{\varepsilon}^d$, distribution solving $\delta\Gamma^d = 0$. By repeating this, one obtains a hygrostrain history at any location in food undergoing drying (coupled solutions of the heat and moisture transfer equations required). A transient state hygrostress, $\boldsymbol{\sigma}^d$, history at any location in food is estimated from the strain history using the constitutive equation (45).

NUMERICAL SOLUTION ALGORITHM

The governing equations, both heat and moisture transfer and strain–stress formation, are solved applying Galerkin finite element method. For this application, a solution domain is subdivided into curved side isoparametric elements, 20 nodes per each element, since an irregular shape may be mapped with a small number of these elements [21, 22].

The following equations of nodal mass transfer potentials and temperatures are derived from equations (35)–(40):

$$\mathbf{A}_{TM}\boldsymbol{\Phi}+\mathbf{A}_{TT}\boldsymbol{\theta}+\mathbf{B}_{TM}\{\partial\boldsymbol{\Phi}/\partial Fo\}+\mathbf{B}_{TT}\{\partial\boldsymbol{\theta}/\partial Fo\} = \mathbf{F}_T \tag{50}$$

$$\mathbf{A}_{MM}\boldsymbol{\Phi}+\mathbf{A}_{MT}\boldsymbol{\theta}+\mathbf{B}_{MM}\{\partial\boldsymbol{\Phi}/\partial Fo\}\mathbf{B}_{MT}\{\partial\boldsymbol{\theta}/\partial Fo\} = \mathbf{F}_M \tag{51}$$

where $\boldsymbol{\theta}$, $\boldsymbol{\Phi}$ and Fo are nodal dimensionless temperature vector, nodal mass transfer potential vector and time, respectively. The coefficient matrices and vectors in equations (50) and (51) are given in the Appendix.

Equations (50) and (51) are nonlinear since all transport properties are dependent on temperature and mass transfer potential. They are solved using a three-time level, stable noniterative method developed by Comini *et al.* [23, 24]. Since this method is not self-starting, Crank–Nicolson method was applied for the first increment (iterative computations required).

Virtual work functional Γ, equation (48), is minimized applying the Galarkin method and summing the resultant expressions over all elements for each time increment:

$$\Gamma^{d} = (1/2)\sum_{e=1}^{n_e}\int_{v_e}\{\varepsilon_i^{d} * \mathrm{C}_{ij}^{d} * \varepsilon_j^{d} - \varepsilon_i^{d} * \mathrm{C}_i^{*d} * \varepsilon_i^{sd}\}\,\mathrm{d}v^{d} \quad (52)$$

where v_e denotes the volume of an element and n_e is the number of elements used to map the solution domain. The incremental displacements at any location in each element are approximated by

$$\Delta\mathbf{U}^{d} = \mathbf{N}\cdot\Delta\mathbf{d}^{d}. \quad (53)$$

Substituting equation (53) into a dimensionless equivalence of equation (29), the incremental strain vector is given by

$$\Delta\boldsymbol{\varepsilon}^{d} = \mathbf{B}^{d}\cdot\Delta\mathbf{d}^{d} \quad (54)$$

where

$$\mathbf{B}^{d} = \mathbf{A}^{d}\cdot\mathbf{N}. \quad (55)$$

Substitution of equation (54) into equation (55) yields

$$\Gamma = (1/2)(\mathbf{d}^{dT} * \mathbf{K}^{d} * \mathbf{d}^{d} - \mathbf{d}^{dT} * \mathbf{R}^{d}) \quad (56)$$

where the stiffness matrix $\mathbf{K}$ and the force vector $\mathbf{R}$ are

$$\mathbf{K}^{d} = \sum_{e=1}^{n_e}\int_{v_e}\mathbf{B}^{dT}\mathbf{C}^{d}\mathbf{B}^{d}\,\mathrm{d}v^{d} \quad (57)$$

$$\mathbf{R}^{d} = \sum_{e=1}^{n_e}\int_{v_e}\mathbf{B}^{dT}\mathbf{C}^{*d} * \boldsymbol{\varepsilon}^{sd}\,\mathrm{d}v^{d}. \quad (58)$$

The variation of equation (56) is

$$\delta\Gamma = \delta[\mathbf{d}^{dT} * \mathbf{K}^{d} * \mathbf{d}^{d}] - \delta[\mathbf{d}^{dT} * \mathbf{R}^{d}]. \quad (59)$$

Setting equation (59) to zero, Γ is minimized:

$$\mathbf{K}^{d} * \mathbf{d}^{d} - \mathbf{R}^{d} = 0. \quad (60)$$

From the definition of the convolution form, equation (60) becomes

$$\int_{\xi=0}^{Fo}\mathbf{K}^{d}(\lambda^{d}(Fo)-\lambda^{d}(\xi))\,\mathrm{d}[\mathbf{d}^{d}(\xi)] = \mathbf{R}^{d}(Fo). \quad (61)$$

Equation (61) is approximated as

$$\sum_{m=0}^{n+1}\mathbf{K}^{d}[\lambda^{d}(Fo_{n+1})-\lambda^{d}(Fo_{m})]\Delta\mathbf{d}^{d}(Fo_{m}) = \mathbf{R}^{d}(Fo_{n+1}). \quad (62)$$

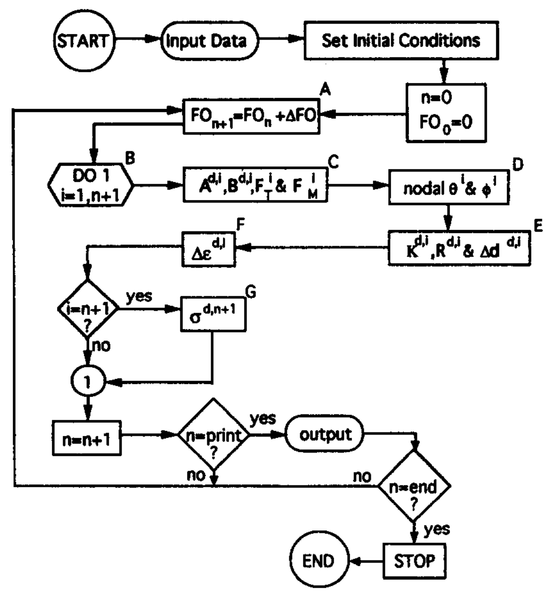

Fig. 1. A bridged flow chart of prepared computer program.

The last increment of displacement is obtained as follows

$$\mathbf{K}^{d}(0)\Delta\mathbf{d}^{d}(Fo_{n+1}) = \mathbf{R}^{d}(Fo_{n+1}) - \sum_{m=0}^{n}\mathbf{K}^{d}(\lambda^{d}(Fo_{n+1}) - \lambda^{d}(Fo_{m}))\Delta\mathbf{d}^{d}(Fo_{m}). \quad (63)$$

The displacement increment at each time step is determined solving equation (63).

The stress is estimated using equation (44) and (54)

$$\boldsymbol{\sigma}^{d}(Fo_{n+1}) = \sum_{m=0}^{n+1}\mathbf{C}^{d}(\lambda(Fo_{n+1})-\lambda(Fo_{m}))\mathbf{B}^{d}\Delta\mathbf{d}^{d}(Fo_{m}) - \sum_{m=0}^{n+1}\mathbf{C}^{d}(\lambda(Fo_{n+1})-\lambda(Fo_{m}))\cdot\Delta\boldsymbol{\varepsilon}^{sd}(Fo_{n+1}). \quad (64)$$

According to equation (63), the current nodal displacements, $\Delta\mathbf{d}$, are determined by numerically integrating $\mathbf{K}^{d}$ with respect to nodal displacement from zero time to the last time step. Additionally, the current nodal hygrostresses are estimated numerically integrating $\mathbf{C}^{d}\,\mathbf{B}^{d}$ with respect to $\Delta\mathbf{d}^{d}$, $\mathbf{C}^{d}$ with respect to stress free strains, equation (64). Since $\mathbf{K}^{d}$, $\mathbf{C}^{d}$ and $\mathbf{B}^{d}$ are dependent on θ and ϕ, directly or indirectly, nodal θ and ϕ histories are required for the integrations.

A computer program was prepared using the numerical solution algorithm, Fig. 1. Initially, $\boldsymbol{\theta}$, $\boldsymbol{\phi}$, $\Delta\mathbf{d}^{d}$ and $\boldsymbol{\sigma}^{d}$ were computed simultaneously at each time step (coupled estimation). However, the estimation of $\boldsymbol{\theta}$ and $\boldsymbol{\phi}$ followed by the estimation of $\Delta\mathbf{d}^{d}$ and $\boldsymbol{\sigma}^{d}$ at each time step (partially uncoupled estimation) produced results virtually identical to the coupled computations with significant computer time saving. Therefore, the partially uncoupled computations were employed in the computer program, blocks C and D for estimating nodal $\boldsymbol{\theta}$ and $\boldsymbol{\phi}$ at the current time and blocks E, F and G for estimating nodal σ^d at the current time. Nodal $\mathbf{K}^d$ histories are required to estimate current nodal $\Delta\mathbf{d}^d$, equation (63), and nodal $\Delta\mathbf{d}^d$ histories are required to estimate current nodal σ^d; equation (64). Therefore, nodal $\mathbf{K}^d$ and $\Delta\mathbf{d}^d$ at each step were stored together with nodal $\boldsymbol{\theta}$ and $\boldsymbol{\phi}$.

EXPERIMENTAL VALIDATION

Triply layered sample shaped samples were prepared from the hydrates of high amylose starch granules (H) and of 1 : 3 mixture of sucrose and high amylose starch granules (S). The initial, overall dimension of each sample was $19.3 \times 15.8 \times 14$mm (length × width × height). Samples were made arranging differently H and S layers. In one arrangement, one 6 mm thick rectangular S plate ($19.3 \times 15.8 \times 6$ mm) was placed between two 4 mm thick rectangular H plates, HSH brick sample. Another had the reversed layer arrangement, SHS brick sample. The initial moisture content and temperature of each sample were 0.2 g water/g dry matter and 25°C, respectively.

A copper–constantan thermocouple made from 36-gauge wires was inserted at the center of a brick of each layer arrangement to monitor a temperature history during drying.

The prepared samples were dried in a 50°C forced air dryer (C. G. Sargent's Sons Corp., Graniteville, MA). Those without the installed thermocouples were taken out periodically from the drier to determine gravimetrically changes in the overall average moisture concentration of each sample (the dry matter of each sample determined by a vacuum oven method [25] upon completing the drying experiment). Additionally, different samples were subjected to different drying processes at the same conditions and taken out to determine the average concentration of the S or H layer after separating it carefully. Other samples were taken out from the drier at 0.2 and 1.0 h of drying. Each sample was bisected across the layer thickness at the midpoint of 14.3 mm (initial size) edge to take pictures of cracks on the bisected surface.

Table 1 shows the drying conditions and physical property values of the samples. The listed values were obtained from Furuta *et al.* [26], Sakai and Hayakawa [18] and Tsukada *et al.* [3]. The values of h_m and h_t are dependent on the sample shape and size and drying conditions. Therefore, they were determined from a separate set of experimental temperature and moisture histories through an optimization method.

Figure 2(a) and (b) shows experimental and theoretical temperature and moisture histories of HSH and SHS samples, respectively. The experimental histories agree well with the respective theoretical histories, especially when one considers difficulty in determining the moisture history of each layer of the composite brick samples. The figures show significant influence of the layer arrangement on the moisture histories, much smaller concentration differences between the

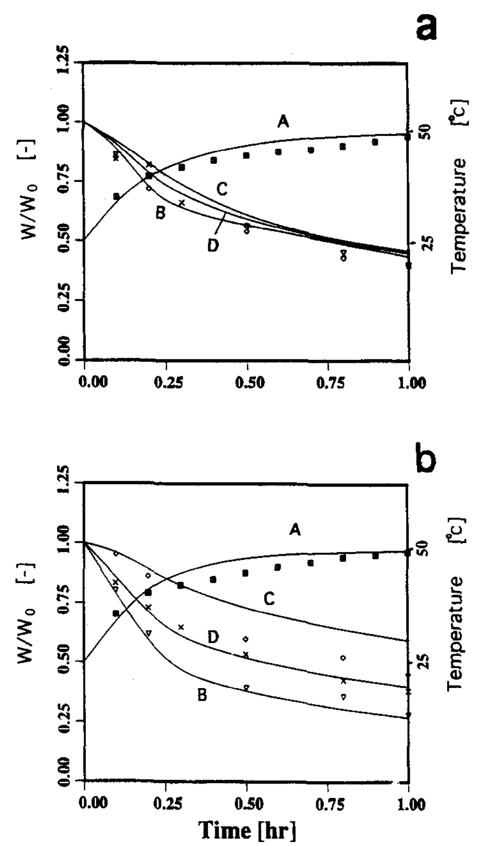

Fig. 2. Moisture concentration and central temperature histories of HSH and SHS brick samples. (a), HSH brick; (b), SHS brick; solid lines are predicted histories and plotted symbols are experimental data. (A) Central temperature; (B) average moisture concentration of outside layers; (C) average concentration of middle layer; (D) overall average concentration solid; ⊠, central temperature; ◇, average concentration of outside layers; ∇, average concentration of middle layer; X, overall average concentration.

outside (H) and middle (S) layers of the HSH sample compared to those for the SHS sample. This is due to interactive influence of a moisture flux (D-flux) due to drying and a flux (I-flux) across the H and S interface due to ϕ difference between H and S.

Figure 3 shows the moisture sorption isotherms of

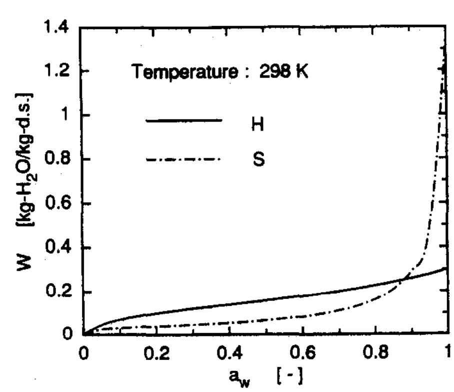

Fig. 3. Moisture sorption isotherms of high amylose starch granules (H) and of H and sucrose 3 : 1 mixture at 25°C.

H and S at 25°C, the initial sample temperature (similar relationship of both isotherms at higher temperatures). It is clear from this figure and equation (9), ϕ of S (ϕ_s) is greater than that of H (ϕ_h) at the zero drying time. Therefore, with the HSH sample, the middle layer (S) lost moisture due to the I-flux flowing out to the outside layer (H) across the interface in addition to the D-flux flowing out directly to the air through its exposed, side surface. This resulted in a large moisture gain by the outside layers from the middle layer, causing a small moisture concentration difference between the middle and outside layers, Fig. 2(a).

With the SHS sample, the initial direction of the I-flux was from the outside layer (S) to the middle layer (H) against the influence of drying while the D-fluxes outflowing directly through the exposed surfaces of both middle and outside layers. This results in a larger moisture concentration difference between the outside and middle layers, Fig. 2(b), because of greater moisture loss by the outside and less moisture loss by the middle compare to the HSH sample.

The drying rate of the outside layers controlled the sample drying rate since their volume was greater than the volume of the middle layer by one third of the latter. Therefore, the SHS sample dried faster than the HSH sample, although the I-flux direction in the former was the outer to middle layer, against the influence of drying, since the outside layers of SHS lost moisture at much greater rates than the outside layers of SHS.

Since the temperature history was monitored at the geometrical center of the middle layer, the history is influenced strongly by the drying rate of this layer (latent heat effect). Therefore, the central temperature of the HSH sample was slightly lower than that of the other sample because the HSH middle layer dried faster than the SHS middle layer.

There are three principal stresses formed at any location in a strained body. These stresses are oriented orthogonally to each other and unidirectional stresses (tensile or compressional stresses) are locally maximum along these orientations.

Figure 4 shows the orientation and magnitudes of two principal stresses estimated at each of 16 selected locations (intersection of each pair of bars) on the one quarter of the 15.8×14 mm bisected plane of the HSH sample, both acted on the plane, at 0.2 and 1 h of drying together with photographs of stress-cracks, on the same plane. The solid line bars represent tensile principal stresses and broken line bars compressional principal stresses. Only one bar is shown when another was too small to show and no bar was shown when both were too small. The third principal stresses, which are not shown, were orthogonal to the plane, i.e. the stresses shown in the figure, and less than those shown. Since the sample is brittle, the maximum tensile principal, stress may be used as a criterion for fracture [27]. Large principal, tensile stresses were formed at 0.2 h in the middle layer, at a location close to the interface and to the exposed side surface. One oriented about 45° from the x-axis and another about 135° from the axis, both about 4800 kN/m^2. Therefore, cracks could be formed at this location. The magnitudes of tensile stresses were reduced greatly at 1.0 h. No cracks of significant sizes are apparent from the photograph taken at 0.2 h. However, the photograph at 1.0 h shows a large crack formed at a location close to the location of the large tensile stress estimated at 0.2 h, the crack extended to the outside layer. Cracks could be formed shortly after 0.2 h since the magnitudes of tensile, stresses were reduced after 0.2 h. The crack extension to the outside layer could be due to crack propagation which was not addressed in the present study.

Figure 5 shows simulation results and photographs for the SHS samples. The maximum tensile, principal stress at 0.2 h was about 60% of the maximum stress in the HSH sample. At 1.0 h, stresses were reduced greatly. Therefore, less cracks would be formed in the SHS compared to the HSH. The photographs show no cracks of significant sizes.

There was no shrinkage in both H and S when $W < 0.2$ g water g dry solid^{-1} as indicted by the shrinkage function in Table 1. Since the initial sample moisture was 0.2 g g^{-1}, there should not be volumetric change in the sample if it is homogeneous. However, with the HSH sample, there was the I-flux from the middle layer (S) to the outside layers (H). Therefore, moisture concentrations became greater than 0.2 g g^{-1} at locations adjacent to the interface in the outside layers according to the simulation. This caused volumetric changes at these locations, resulting in stress formation. Similar simulation results were obtained with the SHS sample.

CONCLUSIONS

Governing equations were obtained to simulate transient state, three dimensional heat and moisture transfer and viscoelastic hygrostress formation in a composite body during drying. In these equations, the chemical potential of water in food was used as a mass transfer potential since moisture concentration could not be used because different composite components had different affinities to moisture. These equations were solved numerically by a finite element method subdividing a composite body into 20-nodes isoparametric elements.

Heat and moisture transfer and hygrostress formation were simulated for the layered bricks made from the hydrates of starch powders and of starch powders–sucrose 3 : 1 mixture, which were subjected to forced-air drying. Simulated results agreed favorably with those observed experimentally. Both simulated and observed results show the strong influence of layer-arrangement on moisture transfer and stress formation and slight influence on heat transfer.

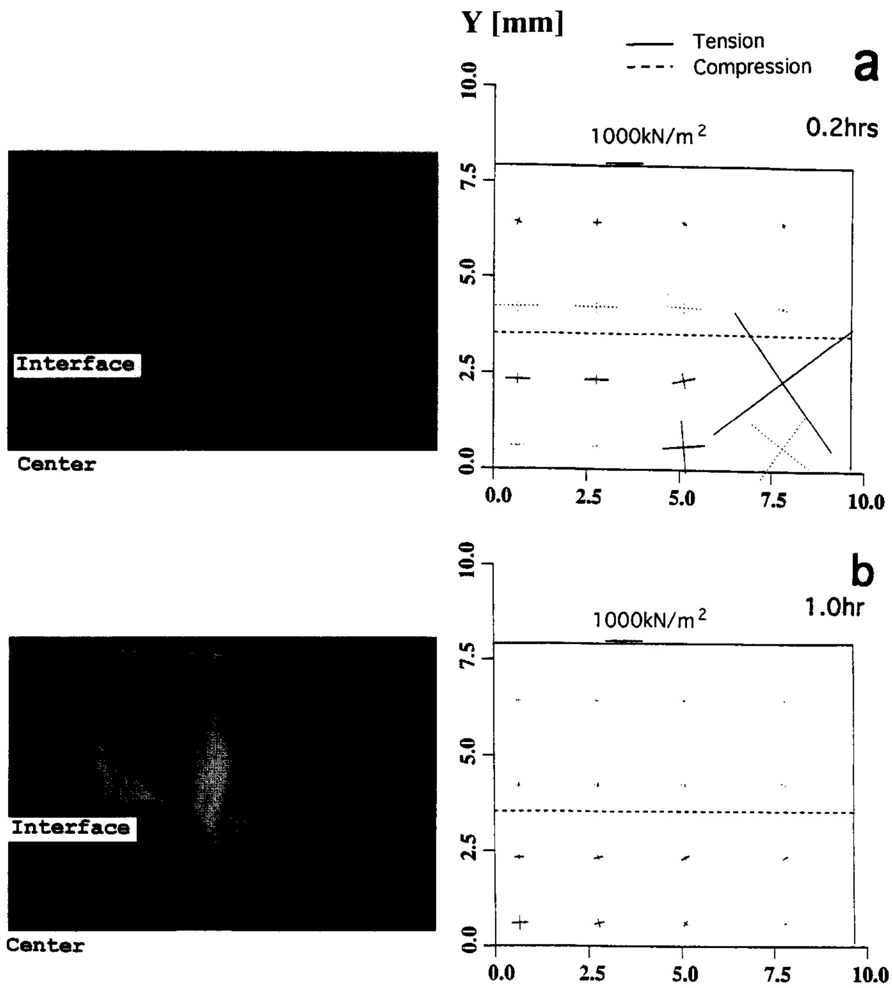

Fig. 4. Estimated two principal stresses at 16 selected locations, specified by intersection of each pair of bars, on one quarter of bisected face of HSH brick and photographed cracks at 0.2 h (a) and 1.0 h (b) of drying. The stress magnitude and orientation are presented by bar-length and bar-orientation, respectively. Solid and broken bars represent tensile and compressional stresses, respectively.

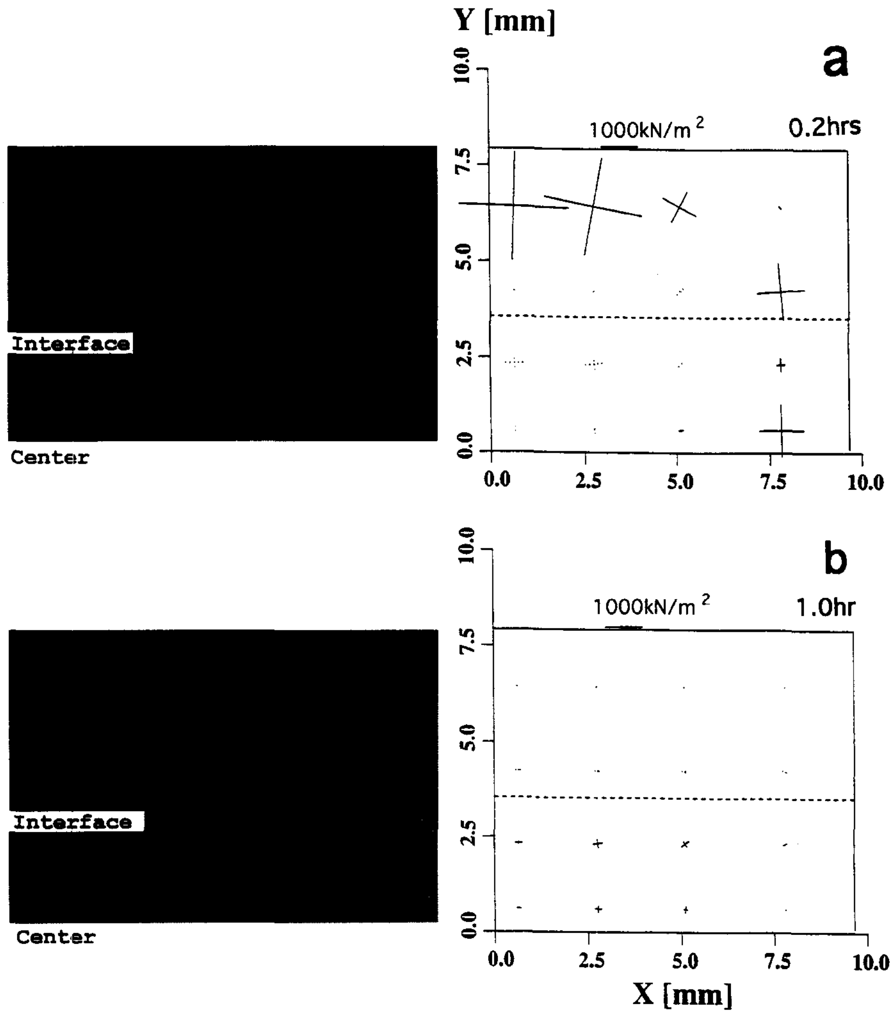

Fig. 5. Estimated two principal stresses at 16 selected locations and observed cracks on one quarter of bisected face of SHS brick at 0.2 h (a) and 1.0 h (b).

Table 1. Drying conditions, transport and physical properties used for the simulation†

Air temperature (T_a)	323 [K]
Initial temperature (T_o)	298 [K]
Initial moisture content (W_o):	0.2 [kg water (kg solid)$^{-1}$]
Relative humidity in air (RH)	0.11
Surface heat transfer coefficient (h_t)	23.2 [W m^{-2} K^{-1}]
Surface mass transfer coefficient (h_m)	8.22×10^{-5} [kg m^{-2} Pa^{-1} s^{-1}]
Volumetric shrinkage coefficient of H (s_v)	$\begin{cases} 1.000+0.601(W-0.2) & \text{for } W \geqslant 0.2 \\ 1.00 & \text{for } W < 0.2 \end{cases}$
Volumetric shrinkage coefficient of S (S_v)	$\begin{cases} 1.000+0.737(W-0.2) & \text{for } W \geqslant 0.2 \\ 1.00 & \text{for } W < 0.2 \end{cases}$
Moisture diffusivity (D_W)	
$D_W = 1.448 \times 10^{-4}(6.402 \times 10^{-4} + W \times 10^{-3})^2 W^{0.5954} \times \exp[8 \times 10^4(0.147+1/(1+10W))$	$\times (1/323 - 1/(T+273))/8.314]$ [m^2 s^{-1}]
Soret mass diffusivity (D_t)	5.54×10^{-9} [kg m^{-1} s^{-1} K^{-1}]
Pressure mass diffusivity (D_p)	0.0 [s]
Thermal conductivity (k_t)	$0.35+1.16 \times 10^{-3}(T-273)+0.058W/(1+W)$ [W m^{-1} K^{-1}]
Dufour thermal conductivity (k_c)	0.0 [W m^2 kg^{-1}]
Filtrational thermal conductivity (k_p)	0.0 [W m^{-1} Pa^{-1}]
Luikov's phase conversion criteria (ε_L)	$1-W/W_o$
Specific heat (c_p)	$1.90 \times 10^3 - 12.1(T-273)+1.73 \times 10^3 W/(1+W)$ [J kg^{-1} K^{-1}]
Density of H (ρ_s)	$0.603 \times 10^3(1+W)/S_v$ [kg m^{-3}]
Density of S (ρ_s)	$0.741 \times 10^3(1+W)/S_v$ [kg m^{-4}]
Chemical reaction rate (R_j)	0.0 [kg s^{-1}]
Equilibrium moisture content (W_e)	$W_n = \dfrac{W_n E Q a_w}{(1-Qa_w)(1-Qa_w+EQa_w)}$

H	S
$E = 7.198 \times 10^{-4} \exp(3021/T)$,	$E = 1.37 \times 10^{-3} \exp(3021/T)$
$Q = 0.370 \exp(142.1/T)$,	$Q = 0.642 \exp(142.1/T)$
$w_n = 0.07259 \exp(162.6/T)$,	$w_n = 0.02088 \exp(162.6/T)$

Equilibrium vapor pressure on the surface (P)

$$P = (101.3 \times 10^3 \exp[13.087(1-373.15/T_s)] \cdot (a_w \text{ at surface moisture}) \text{ [Pa]}$$

Bulk and shear moduli ($K(t)$, $G(t)$)

$$K(t) = \frac{E(t)}{3(1-2\nu)} \quad G(t) = \frac{E(t)}{2(1+\nu)}$$

$$E(t) = 1.31 \times 10^8 + 2.00 \times 10^8 \exp(-t/3.50 \times 10^2) + 8.27 \times 10^7 \exp(-t/1.43 \times 10^2) \text{ [Pa]}$$

$\nu = 0.35$

$n_s = 1/3$

Moisture shift factor (a_M)	1.0
Temperature shift factor (a_T)	1.0
Stefan–Boltzman constant (β)	5.67×10^{-8} [W m^{-2} K^{-4}]
ϕ_2	0.64

† Applicable to both H and S unless stated otherwise. Property values were from Furuta et al. [26], Sakai and Hayakawa [18] and Tsukada et al. [3].

Acknowledgements—This is publication nos D10103-2-94 and D10535-5-94 of New Jersey Agricultural Experiment Station supported by the Center for Advanced Food Technology (CAFT), State Fund, Hatch Act Fund, National Science Foundation (supercomputer time grant at Pittsburgh Supercomputing Center), Cray Research Inc. (supercomputer time grant at Pittsburgh Supercomputing Center), and Rutgers University Computing Services. The Center for Advanced Food Technology is a New Jersey Commission on Science and Technology.

REFERENCES

1. R. J. Gustafson, D. R. Thompson and S. Sokhansany, Temperature and stress analysis of corn kernel finite element analysis, *Trans. ASAE* **22,** 955–960 (1979).
2. R. N. Misra and J. H. Young, Numerical solution of simultaneous moisture diffusion and shrinkage during soybean drying, *Trans. ASAE* **23,** 1277–1282 (1980).
3. T. Tsukada, N. Sakai and K. Hayakawa, Development of computerized model for strain–stress analysis of food undergoing a simultaneous heat and mass transfer process, *J. Fd Sci.* **56,** 1438–1445 (1991).
4. G. C. Zoerb and C. W. Hall, Some mechanical and rheological properties of grains, *J. Agric. Engng Res.* **5,** 83–92 (1958).
5. P. Chen and R. B. Fridley, Analytical methods for determining viscoelastic constants of agricultural material, *Trans. ASAE* **15,** 1103–1106 (1972).
6. F. L. Herum, J. K. Mensah, H. J. Barre and K. Majidzadeh, Viscoelastic behavior of soybean due to temperature and moisture content, *Trans. ASAE* **22,** 1219–1224 (1979).
7. N. N. Mohsenim, *Physical Properties of Plant and Animal Materials.* Gordon & Breach, New York (1986).

8. J. R. Hammerle, Theoretical analysis of failure in viscoelastic slab subjected to temperature and moisture gradients, *Trans. ASAE* **15**, 960–965 (1972).
9. V. N. M. Rao, Stresses in a Maxwell viscoelastic cylinder due to transient temperature and moisture gradients, *Trans. ASAE* **18**, 1165–1169 (1975).
10. V. N. M. Rao, D. D. Hamann and J. R. Hammerle, Stress analysis of a viscoelastic sphere subjected to temperature and moisture gradients, *J. Agric. Engng Res.* **20**, 283–293 (1975).
11. J. B. Litchfield and M. R. Okos, Prediction of corn kernel stress and breakage induced by drying, tempering and cooking, *Trans. ASAE* **31**, 585–594 (1988).
12. K. Haghighi and L. J. Segerlind, Failure of biomaterials subjected to temperature and moisture gradients using the finite element method—I. Thermo-hydro viscoelasticity, *Trans. ASAE* **31**, 930–937 (1988).
13. K. Haghighi and L. J. Segerlind, Failure of biomaterials subjected to temperature and moisture gradients using the finite element method—II. Stress analysis of an isotropic sphere during drying, *Trans. ASAE* **31**, 938–946 (1988).
14. J. Irudagaraj and K. Haghighi, Stress analysis of viscoelastic material during drying—I. Theory and finite element formation, *Drying Technol.* **11**, 901–927 (1993).
15. J. Irudagaraj, K. Haghighi and R. Stroshine, Stress analysis of viscoelastic materials during drying—II. Application to grain kernels, *Drying Technol.* **11**, 929–959 (1993).
16. T. Furuta and K. Hayakawa, Heat and moisture transfer with thermodynamically interactive fluxes and volumetric changes—I. Mathematical model development and numerical solution, *Trans. ASAE* **35**, 1537–1546 (1992).
17. A. V. Luikov, *Heat and Mass Transfer in Capillary-porous Bodies*, pp. 406–407. Pergamon Press, London (1966).
18. N. Sakai and K. Hayakawa, Two-dimensional, simultaneous heat and moisture transfer in composite food, *J. Fd Sci.* **57**, 475–480 (1992).
19. C. J. Lomauro, A. S. Bakshi and T. B. Labuza, Evaluation of food moisture sorption isotherm equations—I. Fruit and vegetable products, *Lebensmittel-Wiss. Technol.* **18**, 111–117 (1985).
20. S. A. Wainwright, W. D. Biggs, J. D. Currey and J. M. Goslin, *Mechanical Design in Organisms*, p. 25. Princeton University Press, Princeton, NJ (1982).
21. K. H. Huebner, *The Finite Element Method for Engineers*, pp. 182–183. John Wiley, New York (1975).
22. O. C. Zienkiewicz, *The Finite Element Method*, Chap. 8. McGraw-Hill, London (1986).
23. G. Comini, S. D. Guidice, R. W. Lewis and O. C. Zienkiewicz, Finite element solution of non-linear heat conduction problems with special reference to phase change, *Int. J. Numer Meth. Engng* **8**, 613–624 (1974).
24. G. Comini and S. D. Guidice, Thermal aspects of cryosurgery, *ASME J. Heat Trans.* **98**, 543–549 (1976).
25. AOAC, *Official Method of Analysis* (12th Edn). Association of Official Analytical Chemists, Washington, DC (1980).
26. T. Furuta, T. Tsukada and K. Hayakawa, Heat and moisture transfer with thermodynamically interactive fluxes and volumetric changes—III. Computer program and sample simulation, *Trans. ASAE* **35**, 1553–1557.
27. J. C. Jaeger, *Elasticity, Fracture and Flow with Engineering and Geological Applications*, pp. 72–75. Methuen/Science Paperbacks, London (1974).

APPENDIX

The elements of the matrices and vectors in equations (50) and (51) are shown below:

$$\mathbf{A}_{\mathrm{MM}} = \int_{v_{\mathrm{T}}} \left(K_{\mathrm{MMX}} \frac{\partial \mathbf{N}^{\mathrm{T}}}{\partial X} \frac{\partial \mathbf{N}}{\partial X} + K_{\mathrm{MMY}} \frac{\partial \mathbf{N}^{\mathrm{T}}}{\partial Y} \frac{\partial \mathbf{N}}{\partial Y} + K_{\mathrm{MMZ}} \frac{\partial \mathbf{N}^{\mathrm{T}}}{\partial Z} \frac{\partial \mathbf{N}}{\partial Z} \right) \mathrm{d}V \quad \text{(A1)}$$

$$\mathbf{A}_{\mathrm{MT}} = \int_{v_{\mathrm{T}}} \left(K_{\mathrm{MTX}} \frac{\partial \mathbf{N}^{\mathrm{T}}}{\partial X} \frac{\partial \mathbf{N}}{\partial X} + K_{\mathrm{MTY}} \frac{\partial \mathbf{N}^{\mathrm{T}}}{\partial Y} \frac{\partial \mathbf{N}}{\partial Y} + K_{\mathrm{MTZ}} \frac{\partial \mathbf{N}^{\mathrm{T}}}{\partial Z} \frac{\partial \mathbf{N}}{\partial Z} \right) \mathrm{d}V \quad \text{(A2)}$$

$$\mathbf{A}_{\mathrm{TM}} = \int_{v_{\mathrm{T}}} \left(K_{\mathrm{TMX}} \frac{\partial \mathbf{N}^{\mathrm{T}}}{\partial X} \frac{\partial \mathbf{N}}{\partial X} + K_{\mathrm{TMY}} \frac{\partial \mathbf{N}^{\mathrm{T}}}{\partial Y} \frac{\partial \mathbf{N}}{\partial Y} + K_{\mathrm{TMZ}} \frac{\partial \mathbf{N}^{\mathrm{T}}}{\partial Z} \frac{\partial \mathbf{N}}{\partial Z} \right) \mathrm{d}V \quad \text{(A3)}$$

$$\mathbf{A}_{\mathrm{TT}} = \int_{v_{\mathrm{T}}} \left(K_{\mathrm{TTX}} \frac{\partial \mathbf{N}^{\mathrm{T}}}{\partial X} \frac{\partial \mathbf{N}}{\partial X} + K_{\mathrm{TTY}} \frac{\partial \mathbf{N}^{\mathrm{T}}}{\partial Y} \frac{\partial \mathbf{N}}{\partial Y} + K_{\mathrm{TTZ}} \frac{\partial \mathbf{N}^{\mathrm{T}}}{\partial Z} \frac{\partial \mathbf{N}}{\partial Z} \right) \mathrm{d}V + (H_{\mathrm{T}} + \beta_{\mathrm{d}}) \int_{Sa} \mathbf{N}^{\mathrm{T}}\mathbf{N}\,\mathrm{d}S \quad \text{(A4)}$$

$$\mathbf{B}_{\mathrm{MM}} = C_{\mathrm{MM}} \int_{v_{\mathrm{T}}} \mathbf{N}^{\mathrm{T}}\mathbf{N}\,\mathrm{d}v \int_{v_{\mathrm{T}}} \mathbf{N}\,\mathrm{d}V \quad \text{(A5)}$$

$$\mathbf{B}_{\mathrm{MT}} = C_{\mathrm{MT}} \int_{v_{\mathrm{T}}} \mathbf{N}^{\mathrm{T}}\mathbf{N}\,\mathrm{d}V \quad \text{(A6)}$$

$$\mathbf{B}_{\mathrm{TM}} = -C_{\mathrm{TM}} \int_{v_{\mathrm{T}}} \mathbf{N}^{\mathrm{T}}\mathbf{N}\,\mathrm{d}V \quad \text{(A7)}$$

$$\mathbf{B}_{\mathrm{TT}} = C_{\mathrm{TT}} \int_{v_{\mathrm{T}}} \mathbf{N}^{\mathrm{T}}\mathbf{N}\,\mathrm{d}V \int_{v_{\mathrm{T}}} \mathbf{N}^{\mathrm{T}}\mathbf{N}\,\mathrm{d}V \quad \text{(A8)}$$

$$\mathbf{F}_{\mathrm{M}} = -H_{\mathrm{M}}(\psi - 1) \int_{Sa} \mathbf{N}^{\mathrm{T}}\,\mathrm{d}S + R_{\mathrm{j}}^{\mathrm{d}} \int_{V_{\mathrm{T}}} \mathbf{N}^{\mathrm{T}}\,\mathrm{d}V \quad \text{(A9)}$$

$$\mathbf{F}_{\mathrm{T}} = \{H_{\mathrm{T}} + \beta_{\mathrm{d}} - (1 - \varepsilon_{\mathrm{L}})\,H_{\mathrm{M}}\Delta H_{\mathrm{v}}^{\mathrm{d}}(\psi - 1)\} \int_{Sa} \mathbf{N}^{\mathrm{T}}\,\mathrm{d}S + \sum \Delta H_{\mathrm{rj}}^{\mathrm{d}} \mathbf{R}_{\mathrm{j}}^{\mathrm{d}} \int_{v_{\mathrm{T}}} \mathbf{N}^{\mathrm{T}}\,\mathrm{d}V. \quad \text{(A10)}$$